

Insight into the structure-property relation of UO₂ nanoparticles

Evgeny Gerber^{a,b,c}, Anna Yu. Romanchuk^c, Stephan Weiss^b, Stephen Bauters^{a,b}, Bianca Schacherl^d, Tonya Vitova^d, René Hübner^b, Salim Shams Aldin Azzam^b, Dirk Detollenaere^{e,f}, Dipanjan Banerjee^{f,g}, Sergei M. Butorin^h, Stepan N. Kalmykov^c and Kristina O. Kvashnina^{a,b,c*}

Highly crystalline UO₂ nanoparticles (NPs) with sizes of 2-3 nm were produced by fast chemical deposition of uranium(IV) under reducing conditions at pH 8-11. The particles were then characterized by microscopic and spectroscopic techniques including high-resolution transmission electron microscopy (HRTEM), X-ray diffraction (XRD), high-energy resolution fluorescence detection (HERFD) X-ray absorption spectroscopy at the U M₄ edge and extended X-ray absorption fine structure (EXAFS) spectroscopy at the U L₃ edge. The results of this investigation show that despite U(IV) being the dominant oxidation state of the freshly prepared UO₂ NPs, they oxidize to U₄O₉ with time and under the X-ray beam, indicating the high reactivity of U(IV) under these conditions. Moreover, it was found that the oxidation process of NPs is accompanied by their growth in size to 6 nm. We highlight here the major differences and similarities of the UO₂ NPs properties with PuO₂, ThO₂ and CeO₂ NPs.

Introduction

Uranium dioxide remains one of the most essential uranium compounds due to its application as a nuclear fuel in most of the commercial nuclear reactors worldwide.¹ Structural chemistry and physics of the U/O system are very complicated but highly important for reactor performance, spent nuclear fuel storage and its further geological disposal. While bulk UO₂ has been intensively studied, it is still not clear if the investigated properties persist the same at the nanoscale.^{2,3} It is known that actinide (An) nanoparticles (NPs) form aggregates of various sizes.^{4,5} In particular, UO₂ NPs may be formed by redox reactions from either the reduction of U(VI) by γ -irradiation,⁶ minerals,⁷⁻¹⁰ microorganisms,¹¹⁻¹⁷ redox-active chemicals¹⁸ or due to corrosion of metallic U being in contact with water.^{4,19,20} It can also be formed via hydrolysis of U(IV) solutions²¹⁻²³ or by decomposition of U(IV) compounds.²⁴

Under environmental conditions, uranium mineral NPs are found to be ubiquitous and have been identified in a number of studies.^{7,25-28} As highly-hydrolysable cation, U(IV) migrates predominantly in the form of pseudo-colloids and intrinsic colloids rather than in the soluble complexed form. UO₂ NPs formed as a result of bacteria mediated redox reactions have

an influence on U migration in the far-field conditions of repositories. Accidental (like Chernobyl and Fukushima) and routine releases of radionuclides into the environment result in the formation of U oxide NPs.²⁹⁻³² It has also been shown that the dissolution of spent nuclear fuel may result in the formation of UO₂ NPs that should be taken into account in the performance assessment of repositories,³³ considering that conditions in deep geological repositories are expected to be reducing.

The peculiarities of nanoscale objects affect their properties.² Nanoscale UO₂ is readily oxidized with the formation of UO_{2+x}, while the crystal structure does not significantly alter.³⁵⁻³⁷ Similar AnO_{2+x} NPs with a structure close to bulk AnO₂ were also observed for plutonium,³⁸ which is not surprising as both UO₂ and PuO₂ are isostructural to the fluorite-type fcc structure with a very similar lattice parameter. However, recent publications show that PuO₂ NPs do not contain other oxidation states except for Pu(IV)^{39,40} and their structural properties are close to the bulk. Similar predictions were made for CeO₂ NPs, with the suggestion that CeO_{2-x} NPs were expected to be predominantly composed of Ce(IV), which can be reduced to Ce(III).⁴¹ Later, the absence of the Ce(III) oxidation state was confirmed for NPs even for 2nm particles.^{42,43} This could lead to the assumption that there is a similar trend for all highly-hydrolyzed tetravalent Ln or An cations. However, to the best of our knowledge, the tetravalent oxidation state for UO₂ NPs has never been proven.

The main difference between U and Pu lies in multivalent behaviour. Under oxidizing conditions, PuO₂ is the sole stable oxide, but more than ten stable U binary oxides – UO_{2+x} – are known. Similar to plutonium, CeO₂ is the only stable oxide under oxidizing conditions, however both Ce(IV) and Ce(III) ions may present in solution. Later we briefly compare the differences and similarities of various An and Ln oxide NPs properties, based on the results reported here.

^a The Rossendorf Beamline at ESRF – The European Synchrotron, CS40220, 38043 Grenoble Cedex 9, France.

^b Helmholtz-Zentrum Dresden-Rossendorf (HZDR), Institute of Resource Ecology, PO Box 510119, 01314, Dresden.

^c Lomonosov Moscow State University, Department of Chemistry, 119991 Moscow, Russia.

^d Institute for Nuclear Waste Disposal (INE), Karlsruhe Institute of Technology, P.O. 3640, D-76021 Karlsruhe, Germany

^e Department of Chemistry, X-ray Imaging and Microspectroscopy Research Group, Ghent University, Ghent, Belgium

^f Dutch-Belgian Beamline (DUBBLE), European Synchrotron Radiation Facility, 71 Avenue des Martyrs, CS 40220, 38043 Grenoble Cedex 9, France

^g Department of Chemistry, KU Leuven, Celestijnenlaan 200F, Box 2404, B-3001 Leuven, Belgium

^h Molecular and Condensed Matter Physics, Department of Physics and Astronomy, Uppsala University, P.O. Box 516, Uppsala, Sweden

Experimental

Nanoparticle synthesis

The UO_2 NPs were synthesized from U(IV) aqueous solution by adding ammonia under reducing conditions. Due to the highly sensitive nature of U(IV) towards oxidation, all synthetic procedures, including the preparation of the samples for the following characterization methods were done in a glovebox under nitrogen atmosphere (<10 ppm O_2).

Special care was taken to avoid any contact with oxygen before and during the measurements. U(IV) stock was prepared by galvanostatic reduction of 0.1 M U(VI) in 0.5 M HClO_4 (5 hours, 20 mA). The presence of only U(IV) and the stability of the solution were verified by UV-vis spectrometry (AvaSpec-2048x14, Avantes, Fig. S1). Each U(IV) solution (0.1 M and 0.01 M) was divided into two parts. The first set of aliquots was added to 3 M NH_3 in the volume ratio 1:10 under continuous stirring. The pH of the 3M ammonia solution was 12.5, but the pH slightly decreased due to the interaction with the U(IV) solution, most likely due to hydrolysis reactions. This set of samples was named "0.1 M/0.01 M U(IV) pH > 11". The second set of aliquots of stock U(IV) was added to water in the volume ratio 1:10, after which several drops of 3 M NH_3 were added under continuous stirring to reach pH 8. This set of

for about 2 hours to reach equilibrium. Then, the pH and redox potential of the formed suspensions were measured (Table S1). The UO_2 reference was made by pressing industrially obtained uranium dioxide powder into a pellet followed by sintering at 1700°C under H_2/Ar stream. The industrial uranium dioxide, in its turn, was obtained from UF_6 by the gas-flame method, followed by annealing under reducing conditions at $600 - 650^\circ\text{C}$.⁴⁴ The reference was characterized by X-ray diffraction (XRD) and polarography, the oxygen coefficient of UO_{2+x} was found to be in order of $x=0.001$.

Characterization

Transmission electron microscopy (TEM)

TEM investigations were performed at the Helmholtz-Zentrum Dresden-Rossendorf (HZDR) using an image-C_s-corrected Titan 80-300 microscope (FEI) operated at an accelerating voltage of 300 kV. In particular, selected area electron diffraction (SAED) patterns using a SA aperture of $40\ \mu\text{m}$ and high-resolution TEM (HRTEM) images were recorded.

Powder X-ray diffraction measurements.

Powder X-ray diffraction (PXRD) data were collected at room temperature at the HZDR. XRD diffractograms data were collected with a MiniFlex 600 diffractometer (Rigaku, Tokyo,

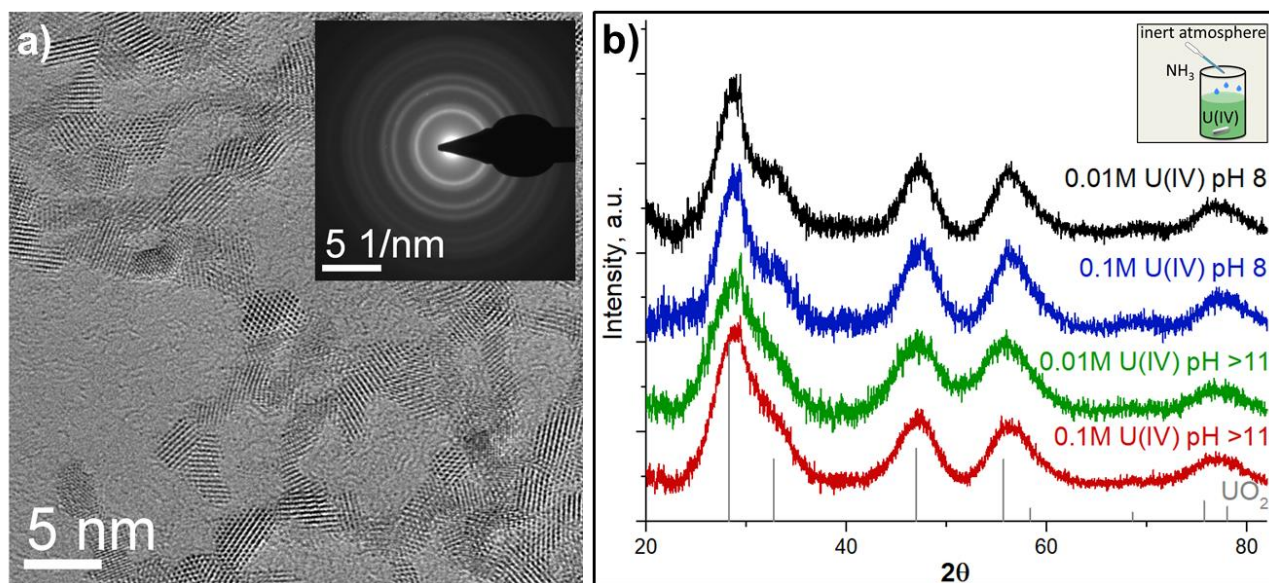


Fig. 1. a) HRTEM image of 0.01M U(IV) pH 8 NPs and corresponding SAED pattern (inset), b) XRD patterns of UO_2 reference and the precipitates from U(IV) with different pH and concentrations. The inset shows the schematic drawing of UO_2 NPs synthesis.

samples was named "0.1M/0.01M U(IV) pH 8". In all syntheses, mixing rate and vessel geometry were maintained constant. The precipitation process for all samples started shortly (within ten minutes) after addition of all reagents. A black precipitate was formed, and the reaction was continued

Japan) equipped with a $\text{Cu K}\alpha$ X-ray source (40 keV/15 mA operation for X-ray generation) and the D/teX Ultra 1D silicon strip detector in the Bragg-Brentano θ - 2θ geometry at a scanning speed of 0.02 degrees per min. The FWHM and peak position were determined with Fityk software.⁴⁵

X-ray absorption near edge structure (XANES) in high-energy resolution fluorescence detection (HERFD) mode at the U M₄ edge and U L₃ extended X-ray absorption fine structure (EXAFS) spectroscopy

The HERFD spectra at the U M₄ edge were collected at the CAT-ACT beamline of the KARA (Karlsruhe research accelerator) facility in Karlsruhe, Germany.⁴⁶ The incident energy was selected using the [111] reflection from a double Si crystal monochromator. Estimated flux at the sample position was in the order of 10⁹ ph/sec at an incident energy of 3.8 keV.⁴⁷ The U HERFD spectra at the M₄ edge were obtained by recording at the maximum intensity of the U M_β emission line (3339.8 eV) as a function of the incident energy. The emission energy was selected using the [220] reflection of one spherically bent Si crystal analyser (1 m bending radius) aligned at 75° Bragg angle. Samples were prepared and sealed in a special argon-filled container at the licensed laboratory of HZDR and were transported to KARA under inert conditions. All samples were mounted in the form of wet pastes within triple holders with 8 μm Kapton window on the front side, serving as first confinement. Three of such holders were mounted in one larger cell, with 13 μm Kapton window on the front side. (second confinement, Fig. S2) The second confinement chamber was constantly flushed with He. The entire spectrometer environment was contained within a He box to improve signal statistics. An energy range from 3710.5 to 3790.5 eV was scanned with a step size down to 0.1 eV using a 1s dwell time per energy point. All samples were tested for short-term beam damage. First an extended timescan (>2 min with 0.1sec step) above the excitation edge was performed before data collection, to monitor any long-term variations in fluorescence signal. Later a preliminary fast HERFD scan (<2 min) was collected and compared with all HERFD data collected per sample. Based on that procedure, the estimated X-ray exposure time has been derived for each sample.

The U L₃ edge (17166 eV) EXAFS spectra were collected at BM26A, the Dutch-Belgium beamline (DUBBLE) at the ESRF (the European Synchrotron) in Grenoble, France.⁴⁸ The energy of the X-ray beam was tuned by using a double-crystal monochromator operating in a fixed-exit mode using a Si(111) crystal pair. Measurements were performed in transmission mode with N₂/He and Ar/He filled ionization chambers. Energy calibration was performed by recording the EXAFS spectrum of the K-edge of metallic Y (~17038 eV) which was collected simultaneously with the sample scans for each sample. The samples were measured at room temperature using a double-confined, heat-sealed polyethylene holder. Energy calibration, averaging of the individual scans, EXAFS data extraction and fitting were performed with the software package Demeter.⁴⁹

Results and discussion

Due to chemical reactivity, the ideal structure of UO₂ can be easily perturbed (even in the bulk crystal).^{35,50,51} The particle size distribution and crystallinity could also differ

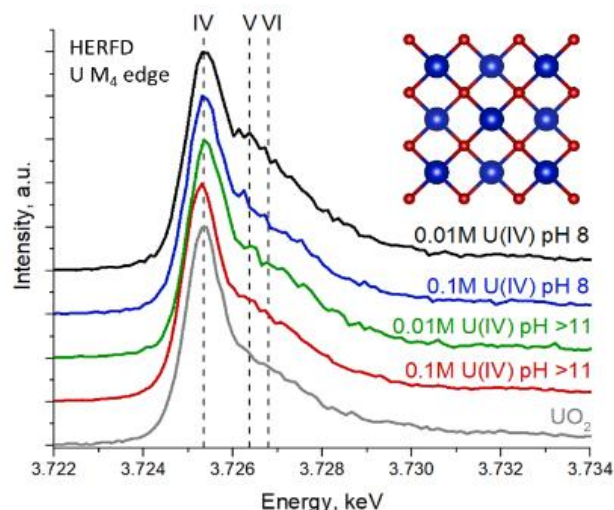


Fig. 2. U M₄ HERFD experimental data recorded for the four UO₂ NPs samples and compared to a UO₂ reference.

depending on the synthesis route^{6,11,52–54}. The HRTEM data reported in Fig. 1a and Fig S3 confirm that regardless of U(IV) concentration and pH conditions, similar NPs are formed (with respect to their size distribution and crystallinity). A comparison of the SAED patterns (Fig. 1a and Fig. S3 (insets)) and diffractograms from XRD measurements (Fig. 1b) with bulk UO₂ show that the crystalline structure of the NPs is similar to that of bulk UO₂ (ICDD 03-065-0285). However, the diffraction peaks are broad, indicating the nanosize dimensions of the samples. The crystallite size was estimated from XRD with Scherrer's equation and found to be similar for all samples, varying in the range of 1.7–2.5 nm (Table S2) with respect to the fact that Scherrer's equation is supposed to give information about coherent domains rather than crystallites. Nevertheless, the diffraction peaks of NPs obtained at pH 8 are slightly narrower than those for pH >11, indicating that pH has a small but notable effect on the NP size. It was unexpected as previous research showed that synthesis conditions highly impact the UO₂ shape and size. For example, Hu and coauthors⁵⁵ made UO₂ in the form of NPs, nanoribbons and nanowires, changing the precursor/organic solvent ratio and temperature. There are many other examples, where the size of the obtained UO₂ NPs varied from several nm up to several microns depending on the synthesis route (radiolytic reduction, organic precursor-assisted syntheses, U(IV) hydrolysis, biogenic reduction etc.) as well as starting precursors and reaction conditions.^{8,13,52–54,56–63} Our HRTEM results (Table S2) also confirm the nanosize of crystallites.

For U–O systems, the number of stoichiometric binary oxides and solid solutions with various compositions are known. Uranium upon oxidation may form various oxides with mixed oxidation states of U (like U₂O₅, U₃O₇, U₄O₉, U₃O₈).^{64,65} The fluorite structure of UO₂ can accommodate a large amount of excess oxygen up to UO_{2.25}, therefore XRD, giving information about coherent scattering domains, is generally less sensitive to this kind of alterations. In other words, the XRD patterns of U₄O₉ and UO₂ are very similar and the presence of those species in UO₂ NPs cannot be detected by

XRD (Fig. S4). Further oxidation of $\text{UO}_{2.25}$ (U_4O_9) may lead to the formation of UO_{2+x} oxides with $0.25 < x \leq 0.33$ accompanied by a changing of the crystal structure. Subsequent oxidation may proceed through the formation of $\text{UO}_{2.5}$ (U_2O_5) and $\text{UO}_{2.67}$ (U_3O_8) until UO_3 is formed.

To further complicate matters, there is a peak broadening effect for NPs in XRD, making reliable analysis nearly impossible, especially in the case of extremely small NPs. That is where synchrotron-based high-energy resolution fluorescence detection (HERFD) X-ray absorption spectroscopy at the U M_4 edge really comes in use. Thanks to its high sensitivity, it can easily detect even the tiniest oxidation state impurities, which are present in many uranium oxides (U_4O_9 , U_3O_8 , U_3O_7).^{9,10,46,66–69} The HERFD method at the An M_4 edge probes An 3d-5f electronic transitions and is thus highly effective for the detection of the 5f electron configuration and for oxidation state identification.^{9,10,39,40,46,66} Moreover, the shapes of the recorded data on various mixed uranium oxides are so distinct^{66,67} that recorded HERFD spectra on uranium systems can be straightforwardly analyzed by a fingerprint approach to detect the presence of $\text{U}_4\text{O}_9/\text{U}_3\text{O}_8$ impurities in UO_2 NPs.

Fig. 2 shows the U M_4 edge measurements on four UO_2 NP samples compared to the spectrum of the UO_2 reference. All spectral features of UO_2 NPs are very similar, corresponding to those of the UO_2 reference, thus confirming the results from XRD and HRTEM. The shape of the main absorption peak in the HERFD spectrum of UO_2 reference shows an asymmetric profile, which was observed before,⁶⁶ however for NP spectra the asymmetry of the peak increases, leading to a high-energy shoulder (Fig. S5). It is expected that the asymmetry of the peak originated from partial oxidation and the presence of oxidized uranium species. However, the theoretical calculations of the U(IV) M_4 HERFD spectra (c.f. SI, Fig. S6) show that nanoscale distortion or even different coordination environment has a strong correlation with the high-energy shoulder in U M_4 HERFD. It is not easy to distinguish between the influence of the presence of higher oxidation state in NPs and the distortion contributions to the asymmetry of the peak. However, theoretical results clearly indicate that the distortion

at the surface and random changes of the coordination number for surface atoms will affect the intensity (increase and decrease) of the higher energy U M_4 HERFD shoulder. Regardless of the asymmetry origin, one can conclude that U(IV) is the dominant oxidation state for UO_2 NPs. To the best of our knowledge, this has never been shown and reported for UO_2 NPs at the high sensitivity that HERFD gives for redox speciation.

The crystallinity of the NPs was investigated for structural disorder by uranium L_3 -edge EXAFS studies (c.f. Fig. S7, Table S3). EXAFS is actively used for uranium^{8,10,63,68,70} to investigate the local chemical environment. It has also been used previously to determine the oxidation state of uranium due to the different U(X)-O bond length (where X is the oxidation state of uranium) and static disorder contributions. Our U L_3 -EXAFS data and shell fit results indicate a UO_2 -like structure, with characteristic distances 2.33 Å and 3.85 Å for U-O and U-U, respectively (Fig. S7). The absence of other shorter or longer U-O distances suggests that there is no need to invoke different U oxidation states or a substantially different structure (e.g. U_4O_9 or U(V)-O). However, the reduced CN for the U-O shell and high Debye-Waller factors are suggestive of particle-size effect and static and thermal disorders, which was previously observed on similar particles.^{8,9,13,63,71}

Taking into account: 1) the significant disorder revealed by EXAFS and 2) the theoretical prediction of the distortion effects on the high-energy shoulder of the U M_4 HERFD spectra, surface distortion might be the predominant reason for the experimental observation of the intensity variation of the high-energy shoulder in U M_4 HERFD data between various UO_2 NPs.

Reactivity of the UO_2 NPs

The reactivity of UO_2 NPs under different conditions was studied previously. It was found, that sintering leads to NP growth.^{6,13} Rath et al. found that UO_2 NPs obtained with γ -irradiation oxidize in several hours under air conditions, while Singer et al. and Wang et al. did not find any changes after 2 months ageing or several days of air exposure.^{11,53,60} However,

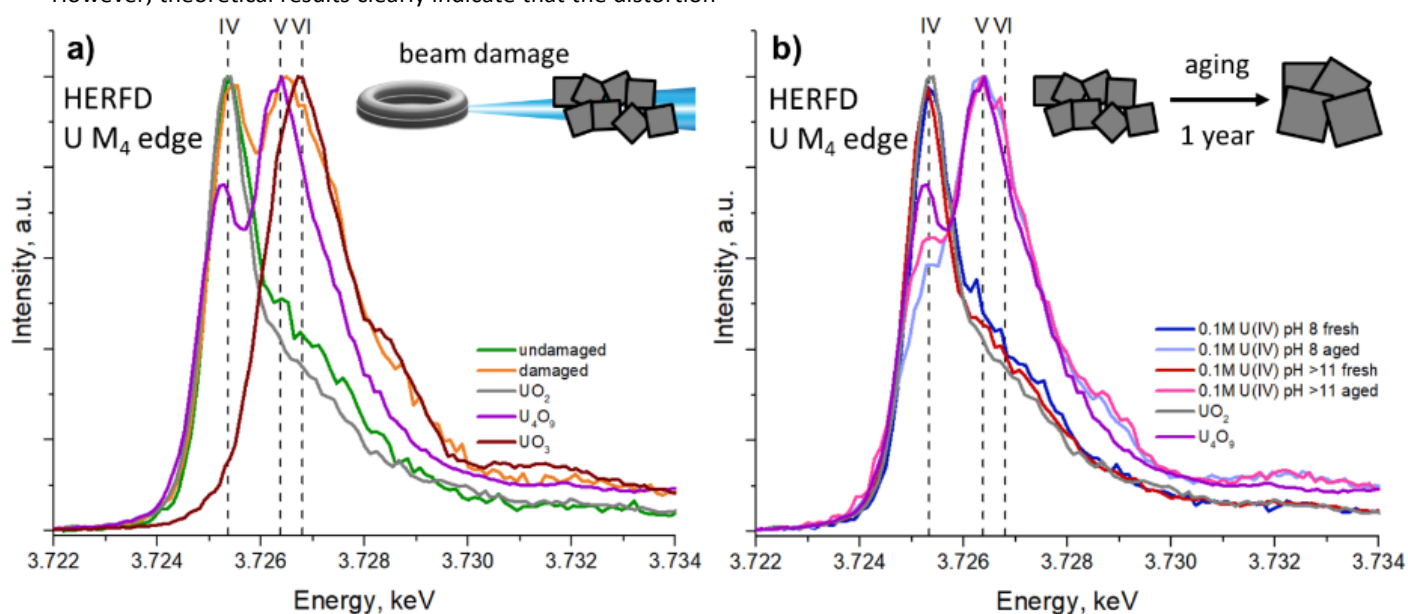


Fig. 3. HERFD M_4 edge spectra: a) for 0.01M U(IV) pH >11 before and after beam damage with references. b) for fresh and 1-year-aged 0.1M samples with references. The HERFD spectra of the UO_3 and U_4O_9 references have been reproduced from data, reported by Leinders et al and have shown here for clarity.⁶⁰

visual observations of the change in residue colour by UV-vis spectroscopy or the U L₃ edge XANES (used in previous studies) may not be sufficient to detect other oxidation states of uranium.

Here we investigate in detail the reactivity and phase stability of synthesized UO₂ NPs. First, we noticed the impact of the synchrotron X-ray beam on the freshly synthesized materials. In order to verify the damage of samples by X-ray irradiation, all samples were scanned several times at the exact same position to examine how the beam exposure affects the samples. Fig. 3a shows the average of the first U M₄ spectra scans on UO₂ NPs synthesized from 0.01M U(IV) pH >11 and its comparison with the last scans after 45-60 minutes of X-ray exposure. With each subsequent scan (which takes 5 min) the shoulder of the HERFD high-energy side increases and can even be resolved as an individual component, indicating the partial oxidation of the sample to U(V) and U(VI). Other samples were oxidized under exposure as well, leading to the conclusion that beam exposure is responsible for uranium oxidation in NPs. In order to obtain data on freshly made materials, HERFD measurements have been made on newly synthesized UO₂ NPs (reported in Fig. 2), with a short X-ray exposure time (15 min in total over several scans) on samples sealed in a special inert gas-filled container (more info is given in experimental section and SI).

The recorded U M₄ HERFD data on oxidized UO₂ NPs are reported in Fig.3 and compared to the spectra of UO₂, U₄O₉ and UO₃ (reproduced from Leinders et al.⁶⁷). It should be noted that despite the longer duration of L₃-edge EXAFS measurements beam damage does not take place in that case due to the lower unfocused beam intensity, compared to M₄-edge HERFD measurements. Several scans made on the same sample position were reproducible and oxidation (or significant differences from UO₂ structure) was not detected.

Moreover, the stability of NPs over time has also been studied. Two samples synthesized from 0.1M U(IV) concentrations were kept as wet pastes under inert conditions and ambient temperature for a year in closed 2mL plastic tubes with a tiny amount of water left after washing the NPs. Afterwards these samples were analysed with HRTEM, XRD and M₄ edge HERFD techniques. It was found that the size of NPs increases (Table S2, Fig. S8-9) after aging (likely, due to the dissolution-precipitation processes⁵⁷), while partial oxidation was observed by HERFD (Fig. 3b). A rise of U(V) contribution in the damaged NPs is shown (Fig. 3a), though it is clear by the difference in peak intensity ratios that the NPs have not fully converted to pure U₄O₉. Bulk U₄O₉ has equal amounts of U(IV) and U(V), yet the peak intensities in HERFD are not the same due to the different probability of the absorption process, i.e. different absolute absorption cross sections of U(IV) and U(V).⁶⁷ Therefore, a significant amount of U(IV) is still retained in our damaged samples. The HERFD spectra on the aged NPs show higher contribution of the U(V) for compare to U(IV). Overall, it leads to the conclusion that small NPs oxidize to U₄O₉ and grow up to 6 nm over time. The size of 6 nm was determined by XRD data and is in agreement with HRTEM size estimations (Table S2).

The strong influence of the X-ray beam and the aging behaviour of the UO₂ NPs are clear evidences of the low stability of the samples; therefore, special care must be taken to avoid sample oxidation and destructive effects of the X-ray beam. The reasonable solution is to keep samples under reducing conditions as long as possible before performing any experiments, to record relatively quick scans and to choose new sample positions for every scan to limit sample exposure. Measurements under cryogenic conditions might also overcome the issue of beam damage, but this has not been tested yet on the UO₂ NPs.

Comparison between various An and Ln oxide NPs

Tetravalent cations (Cat) undergo extensive hydrolysis accompanied by the formation of mono- and oligomeric species. Eventually CatO₂ NPs originate from aqueous solutions. Besides uranium, the formation of small (2-4 nm) crystalline NPs was observed for cerium,⁴³ thorium,⁷² neptunium⁷³ and plutonium.⁷⁴ Dioxides of these elements demonstrate similar crystallographic properties: fluorite-type structure with similar lattice parameter. However, the redox properties of these elements are different. Thorium is redox inactive, while Ce, U, Np and Pu may be present in different oxidation states. The correlation between UO₂ and PuO₂ NPs is of high interest as both U(IV) and Pu(IV) are mobile in their colloid forms.^{5,75,76} The redox conditions in deep geological repositories are expected to be reducing. Therefore, U(IV), being stable under these conditions, could be a reference for Pu(IV) as well, due to the similarities in An(IV) ionic radii and crystallographic properties of their dioxides. Our investigation shows that there are many resemblances between these An(IV) NPs. It was shown³⁹ that neither super stoichiometric AnO_{2+x} nor other higher oxide phases are present in PuO₂ NPs though it could be expected due to the stability of Pu(IV) under these conditions. Similar behaviour can be predicted for NpO₂ NPs, however, to the best of our knowledge the presence of other oxidation states in NpO₂ NPs has not been studied yet by HERFD method.

Contrariwise to Pu and especially Np, Ce(III) is stable in aqueous solutions, therefore, one can expect Ce(III) is present in the hydrolysis products. Nevertheless, it was found^{42,43}, that CeO₂ NPs do not contain even slight amounts of Ce(III), leading to the conclusion that CatO₂ NPs formed by fast chemical deposition retain Cat(IV) as the dominating oxidation state regardless of their redox affinity. In this study we confirmed, that it is also valid for UO₂ NPs, synthesized by fast chemical deposition method under pH 8-11. Those results do not include the possibility that the formation of other phases or other oxidation states takes place under different synthesis conditions.

Conclusions

It is reasonable to believe that the properties of UO₂ in bulk and at the nanoscale are different. Due to a larger surface-to-volume ratio, UO₂ NPs are expected to be more reactive and,

therefore, to exist as UO_{2+x} , with some of the U oxidized at the surface.^{35–37} However, it was found that U(IV) is the dominant oxidation state of the UO_2 NPs, synthesized by fast chemical deposition method at pH 8–11, but their stability is significantly lower than bulk- UO_2 in terms of time and oxidation sensitivity. They are easily oxidized not only in the air but also slowly under inert conditions or during X-ray exposure. Therefore, special care has to be taken while investigating reactions with UO_2 NPs and their properties.

The electronic and local structure of the freshly synthesized UO_2 NPs in size of 2–3 nm was revealed by combination of the U L_{3-} edge EXAFS, U M_{4-} edge HERFD, XRD and HRTEM methods. We show here that the structural and electronic properties of fresh ultra-small UO_2 NPs (2–3 nm) are similar to bulk UO_2 when inert or reducing conditions restrictions are maintained. It was found that high reactivity of UO_2 NPs in time and under X-ray beam exposure leads to the formation of the U_4O_9 species complemented by the growth of the NP size to 6 nm. We believe that these findings are beneficial to the fundamental understanding of nuclear fuels and tailoring the functionality of UO_2 since most previous studies focus on large-bulk UO_2 .

Conflicts of interest

There are no conflicts to declare.

Acknowledgements

This research was funded by European Commission Council under ERC [grant N759696]. E.G. acknowledges support from RFBR (project number No. 19-33-90127). S.N.K. acknowledges support by the Russian Ministry of Science and Education under grant № 075-15-2019-1891. S.M.B. acknowledges support from the Swedish Research Council (Grant 2017-06465). Authors thank HZDR for the beamtime at CAT-ACT beamline of KARA. Moreover, we acknowledge the help of J. Rothe, A. Beck, J. Galanzew and T. Prüßmann at CAT-ACT beamline of KARA during the HERFD experiment at the U M_4 edge. Furthermore, the use of the HZDR Ion Beam Centre TEM facilities is acknowledged.

References

- 1 R. C. Ewing, Long-term storage of spent nuclear fuel, *Nat. Mater.*, 2015, **14**, 252–257.
- 2 M. F. Hochella, D. W. Mogk, J. Ranville, I. C. Allen, G. W. Luther, L. C. Marr, B. P. McGrail, M. Murayama, N. P. Qafoku, K. M. Rosso, N. Sahai, P. A. Schroeder, P. Vikesland, P. Westerhoff and Y. Yang, Natural, incidental, and engineered nanomaterials and their impacts on the Earth system, *Science.*, 2019, **363**, eaau8299.
- 3 H. Wu, Y. Yang and Y. C. Cao, Synthesis of Colloidal Uranium–Dioxide Nanocrystals, *J. Am. Chem. Soc.*, 2006, **128**, 16522–16523.
- 4 T. S. Neill, K. Morris, C. I. Pearce, L. Abrahamsen-Mills, L. Kovarik, S. Kellet, B. Rigby, T. Vitova, B. Schacherl and S. Shaw, Silicate stabilisation of colloidal UO_2 produced by uranium metal corrosion, *J. Nucl. Mater.*, 2019, **526**, 151751.
- 5 S. N. Kalmykov and M. A. Denecke, Eds., *Actinide Nanoparticle Research*, Springer Berlin Heidelberg, Berlin, Heidelberg, 2011.
- 6 T. M. Nenoff, B. W. Jacobs, D. B. Robinson, P. P. Provencio, J. Huang, S. Ferreira and D. J. Hanson, Synthesis and Low Temperature In Situ Sintering of Uranium Oxide Nanoparticles, *Chem. Mater.*, 2011, **23**, 5185–5190.
- 7 J. R. Bargar, K. H. Williams, K. M. Campbell, P. E. Long, J. E. Stubbs, E. I. Suvorova, J. S. Lezama-Pacheco, D. S. Alessi, M. Stylo, S. M. Webb, J. A. Davis, D. E. Giammar, L. Y. Blue and R. Bernier-Latmani, Uranium redox transition pathways in acetate-amended sediments, *Proc. Natl. Acad. Sci.*, 2013, **110**, 4506–4511.
- 8 E. J. O’Loughlin, S. D. Kelly, R. E. Cook, R. Csencsits and K. M. Kemner, Reduction of Uranium(VI) by Mixed Iron(II)/Iron(III) Hydroxide (Green Rust): Formation of UO_2 Nanoparticles, *Environ. Sci. Technol.*, 2003, **37**, 721–727.
- 9 I. Pidchenko, K. O. Kvashnina, T. Yokosawa, N. Finck, S. Bahl, D. Schild, R. Polly, E. Bohnert, A. Rossberg, J. Göttlicher, K. Dardenne, J. Rothe, T. Schäfer, H. Geckeis and T. Vitova, Uranium Redox Transformations after U(VI) Coprecipitation with Magnetite Nanoparticles, *Environ. Sci. Technol.*, 2017, **51**, 2217–2225.
- 10 Z. Pan, B. Bártoová, T. LaGrange, S. M. Butorin, N. C. Hyatt, M. C. Stennett, K. O. Kvashnina and R. Bernier-Latmani, Nanoscale mechanism of UO_2 formation through uranium reduction by magnetite, *Nat. Commun.*, 2020, **11**, 4001.
- 11 D. M. Singer, F. Farges and G. E. Brown, in *AIP Conference Proceedings*, AIP, 2007, vol. 882, pp. 277–279.
- 12 Y. Suzuki, S. D. Kelly, K. M. Kemner and J. F. Banfield, Nanometre-size products of uranium bioreduction, *Nature*, 2002, **419**, 134–134.
- 13 D. M. Singer, F. Farges and G. E. Brown, Biogenic nanoparticulate UO_2 : Synthesis, characterization, and factors affecting surface reactivity, *Geochim. Cosmochim. Acta*, 2009, **73**, 3593–3611.
- 14 M. I. Boyanov, K. E. Fletcher, M. J. Kwon, X. Rui, E. J. O’Loughlin, F. E. Löffler and K. M. Kemner, Solution and Microbial Controls on the Formation of Reduced U(IV) Species, *Environ. Sci. Technol.*, 2011, **45**, 8336–8344.
- 15 L. Newsome, K. Morris and J. R. Lloyd, The biogeochemistry and bioremediation of uranium and other priority radionuclides, *Chem. Geol.*, 2014, **363**, 164–184.
- 16 J. R. Bargar, R. Bernier-Latmani, D. E. Giammar and B. M. Tebo, Biogenic Uraninite Nanoparticles and Their Importance for Uranium Remediation, *Elements*, 2008, **4**, 407–412.
- 17 L. Newsome, K. Morris, D. Trivedi, N. Atherton and J. R. Lloyd, Microbial reduction of uranium(VI) in sediments of different lithologies collected from Sellafield, *Appl. Geochemistry*, 2014, **51**, 55–64.
- 18 K.-U. Ulrich, A. Singh, E. J. Schofield, J. R. Bargar, H. Veeramani, J. O. Sharp, R. Bernier-Latmani and D. E.

- Giammar, Dissolution of Biogenic and Synthetic UO₂ under Varied Reducing Conditions, *Environ. Sci. Technol.*, 2008, **42**, 5600–5606.
- 19 E. L. Fuller, N. R. Smyrl, J. B. Condon and M. H. Eager, Uranium oxidation: Characterization of oxides formed by reaction with water by infrared and sorption analyses, *J. Nucl. Mater.*, 1984, **120**, 174–194.
- 20 M. D. Kaminski, N. M. Dimitrijevic, C. J. Mertz and M. M. Goldberg, Colloids from the aqueous corrosion of uranium nuclear fuel, *J. Nucl. Mater.*, 2005, **347**, 77–87.
- 21 G. Rousseau, M. Fattahi, B. Grambow, F. Boucher and G. Ouvrard, Coprecipitation of thorium with UO₂, *Radiochim. Acta*, 2002, **90**, 523–527.
- 22 T. Fanghänel and V. Neck, Aquatic chemistry and solubility phenomena of actinide oxides/hydroxides, *Pure Appl. Chem.*, 2002, **74**, 1895–1907.
- 23 V. Neck and J. I. Kim, Solubility and hydrolysis of tetravalent actinides, *Radiochim. Acta*, 2001, **89**, 1–16.
- 24 O. Walter, K. Popa and O. D. Blanco, Hydrothermal decomposition of actinide(IV) oxalates: a new aqueous route towards reactive actinide oxide nanocrystals, *Open Chem.*, 2016, **14**, 170–174.
- 25 P. Liu, X. Luo, M. Wen, J. Zhang, C. Zheng, W. Gao and F. Ouyang, Geoelectrochemical anomaly prospecting for uranium deposits in southeastern China, *Appl. Geochemistry*, 2018, **97**, 226–237.
- 26 R. M. Hazen, R. C. Ewing and D. A. Sverjensky, Evolution of uranium and thorium minerals, *Am. Mineral.*, 2009, **94**, 1293–1311.
- 27 M. Schindler, A. J. Lussier, J. Bellrose, S. Rouvimov, P. C. Burns and T. K. Kyser, Mobilization and agglomeration of uraninite nanoparticles: A nano-mineralogical study of samples from the Matoush Uranium ore deposit, *Am. Mineral.*, 2017, **102**, 1776–1787.
- 28 S. Fuchs, D. Schumann, A. E. Williams-Jones and H. Vali, The growth and concentration of uranium and titanium minerals in hydrocarbons of the Carbon Leader Reef, Witwatersrand Supergroup, South Africa, *Chem. Geol.*, 2015, **393–394**, 55–66.
- 29 B. Salbu, K. Janssens, O. C. Lind, K. Proost, L. Gijssels and P. R. Danesi, Oxidation states of uranium in depleted uranium particles from Kuwait, *J. Environ. Radioact.*, 2005, **78**, 125–135.
- 30 P. Pöml and B. Burakov, Study of the redistribution of U, Zr, Nb, Tc, Mo, Ru, Fe, Cr, and Ni between oxide and metallic phases in the matrix of a multiphase Chernobyl hot-particle extracted from a soil sample of the Western Plume, *Radiochim. Acta*, 2018, **106**, 985–990.
- 31 A. Ochiai, J. Imoto, M. Suetake, T. Komiya, G. Furuki, R. Ikehara, S. Yamasaki, G. T. W. Law, T. Ohnuki, B. Grambow, R. C. Ewing and S. Utsunomiya, Uranium Dioxides and Debris Fragments Released to the Environment with Cesium-Rich Microparticles from the Fukushima Daiichi Nuclear Power Plant, *Environ. Sci. Technol.*, 2018, **52**, 2586–2594.
- 32 V. Kashparov, B. Salbu, S. Levchuk, V. Protsak, I. Maloshtan, C. Simonucci, C. Courbet, H. L. Nguyen, N. Sanzharova and V. Zabrotsky, Environmental behaviour of radioactive particles from chernobyl, *J. Environ. Radioact.*, 2019, **208–209**, 106025.
- 33 K. Spahiu, J. Devoy, D. Cui and M. Lundström, The reduction of U(VI) by near field hydrogen in the presence of UO_{2(s)}, *Radiochim. Acta*, **92**, 597–601.
- 34 M. Rovira, S. El Aamrani, L. Duro, J. Giménez, J. de Pablo and J. Bruno, Interaction of uranium with in situ anoxically generated magnetite on steel, *J. Hazard. Mater.*, 2007, **147**, 726–731.
- 35 G. Leinders, J. Pakarinen, R. Delville, T. Cardinaels, K. Binnemans and M. Verwerft, Low-Temperature Oxidation of Fine UO₂ Powders: A Process of Nanosized Domain Development, *Inorg. Chem.*, 2016, **55**, 3915–3927.
- 36 S. Szenknect, D. Alby, M. López García, C. Wang, R. Podor, F. Miserque, A. Mesbah, L. Duro, L. Zetterström Evins, N. Dacheux, J. Bruno and R. C. Ewing, Coffinite formation from UO_{2+x}, *Sci. Rep.*, 2020, **10**, 12168.
- 37 S. R. Spurgeon, M. Sassi, C. Ophus, J. E. Stubbs, E. S. Ilton and E. C. Buck, Nanoscale oxygen defect gradients in UO_{2+x} surfaces, *Proc. Natl. Acad. Sci.*, 2019, **116**, 17181–17186.
- 38 J. M. Haschke, T. H. Allen and L. A. Morales, Reaction of Plutonium Dioxide with Water: Formation and Properties of PuO_{2+x}, *Science*, 2000, **287**, 285–287.
- 39 E. Gerber, A. Y. Romanchuk, I. Pidchenko, L. Amidani, A. Rossberg, C. Hennig, G. B. M. Vaughan, A. Trigub, T. Egorova, S. Bauters, T. Plakhova, M. O. J. Y. Hunault, S. Weiss, S. M. Butorin, A. C. Scheinost, S. N. Kalmykov and K. O. Kvashnina, The missing pieces of the PuO₂ nanoparticle puzzle, *Nanoscale*, 2020, **12**, 18039–18048.
- 40 K. O. Kvashnina, A. Y. Romanchuk, I. Pidchenko, L. Amidani, E. Gerber, A. Trigub, A. Rossberg, S. Weiss, K. Popa, O. Walter, R. Caciuffo, A. C. Scheinost, S. M. Butorin and S. N. Kalmykov, A Novel Metastable Pentavalent Plutonium Solid Phase on the Pathway from Aqueous Plutonium(VI) to PuO₂ Nanoparticles, *Angew. Chemie - Int. Ed.*, 2019, **58**, 17558–17562.
- 41 O. N. Batuk, D. V Szabo, M. A. Denecke, T. Vitova and S. N. Kalmykov, Synthesis and characterization of thorium , uranium and cerium oxide nanoparticles, *Radiochim. Acta*, 2013, **101**, 233–239.
- 42 J.-D. Cafun, K. O. Kvashnina, E. Casals, V. F. Puentes and P. Glatzel, Absence of Ce³⁺ Sites in Chemically Active Colloidal Ceria Nanoparticles, *ACS Nano*, 2013, **7**, 10726–10732.
- 43 T. V. Plakhova, A. Y. Romanchuk, S. M. Butorin, A. D. Konyukhova, A. V. Egorov, A. A. Shiryaev, A. E. Baranchikov, P. V. Dorovatovskii, T. Huthwelker, E. Gerber, S. Bauters, M. M. Sozarukova, A. C. Scheinost, V. K. Ivanov, S. N. Kalmykov and K. O. Kvashnina, Towards the surface hydroxyl species in CeO₂ nanoparticles, *Nanoscale*, 2019, **11**, 18142–18149.
- 44 O. N. Batuk, S. N. Kalmykov, V. G. Petrov, E. V. Zakharova, Y. A. Teterin, A. Y. Teterin, V. I. Shapovalov and M. J. Haire, Neptunium interaction with uranium dioxide in aqueous solution, *J. Nucl. Mater.*, 2007, **362**, 426–430.
- 45 M. Wojdyr, Fityk : a general-purpose peak fitting program, *J. Appl. Crystallogr.*, 2010, **43**, 1126–1128.

- 46 J. Rothe, M. Altmaier, R. Dagan, K. Dardenne, D. Fellhauer, X. Gaona, E. G.-R. Corrales, M. Herm, K. O. Kvashnina, V. Metz, I. Pidchenko, D. Schild, T. Vitova and H. Geckeis, Fifteen Years of Radionuclide Research at the KIT Synchrotron Source in the Context of the Nuclear Waste Disposal Safety Case, *Geosciences*, 2019, **9**, 91.
- 47 A. Zimina, K. Dardenne, M. A. Denecke, D. E. Doronkin, E. Huttel, H. Lichtenberg, S. Mangold, T. Pruessmann, J. Rothe, T. Spangenberg, R. Steininger, T. Vitova, H. Geckeis and J.-D. Grunwaldt, CAT-ACT—A new highly versatile x-ray spectroscopy beamline for catalysis and radionuclide science at the KIT synchrotron light facility ANKA, *Rev. Sci. Instrum.*, 2017, **88**, 113113.
- 48 M. Borsboom, W. Bras, I. Cerjak, D. Detollenaere, D. Glastra van Loon, P. Goedtkindt, M. Konijnenburg, P. Lassing, Y. K. Levine, B. Munneke, M. Oversluizen, R. van Tol and E. Vlieg, The Dutch–Belgian beamline at the ESRF, *J. Synchrotron Radiat.*, 1998, **5**, 518–520.
- 49 B. Ravel and M. Newville, ATHENA, ARTEMIS, HEPHAESTUS: Data analysis for X-ray absorption spectroscopy using IFFFIT, *J. Synchrotron Radiat.*, 2005, **12**, 537–541.
- 50 L. Desgranges, G. Baldinozzi, G. Rousseau, J.-C. Nièpce and G. Calvarin, Neutron Diffraction Study of the in Situ Oxidation of UO₂, *Inorg. Chem.*, 2009, **48**, 7585–7592.
- 51 D. A. Andersson, G. Baldinozzi, L. Desgranges, D. R. Conradson and S. D. Conradson, Density Functional Theory Calculations of UO₂ Oxidation: Evolution of UO_{2+x}, U₄O_{9-y}, U₃O₇, and U₃O₈, *Inorg. Chem.*, 2013, **52**, 2769–2778.
- 52 S. Hasan and T. K. Ghosh, Synthesis of Uranium Oxide Nanoparticles in Aqueous Solutions, *Nucl. Technol.*, 2011, **173**, 310–317.
- 53 Y. Wang, Q. Chen and X. Shen, Preparation of low-temperature sintered UO₂ nanomaterials by radiolytic reduction of ammonium uranyl tricarbonate, *J. Nucl. Mater.*, 2016, **479**, 162–166.
- 54 M. C. Rath, S. Keny and D. B. Naik, Direct Synthesis of UO₂ Nanoparticles in Aqueous Solutions Through Photochemical Method, *J. Nanosci. Nanotechnol.*, 2016, **16**, 9575–9582.
- 55 S. Hu, H. Li, H. Liu, P. He and X. Wang, Nanocrystals of Uranium Oxide: Controlled Synthesis and Enhanced Electrochemical Performance of Hydrogen Evolution by Ce Doping, *Small*, 2015, **11**, 2624–2630.
- 56 A. Leticia Soldati, D. Carolina Lago and M. Oscar Prado, in *Nuclear Materials*, IntechOpen, 2020.
- 57 A. J. Popel, B. T. Tan, T. Gouder, G. I. Lampronti, J. Day, R. Eloirdi, A. Seibert and I. Farnan, Surface alteration evidence for a mechanism of anoxic dissolution of UO₂, *Appl. Surf. Sci.*, 2019, **464**, 376–379.
- 58 L. Balice, D. Bouëxière, M. Cologna, A. Cambriani, J. Vigier, E. De Bona, G. Domenico, C. Kübel, O. Walter and K. Popa, Nano and micro U_{1-x}Th_xO₂ solid solutions : From powders to pellets, *J. Nucl. Mater.*, 2018, **498**, 307–313.
- 59 N. P. Martin, C. Volklinger, N. Henry, X. Trivelli, G. Stoclet, A. Ikeda-Ohno and T. Loiseau, Formation of a new type of uranium poly-oxo cluster {U₃₈} based on a controlled release of water via esterification reaction, *Chem. Sci.*, 2018, **9**, 5021–5032.
- 60 M. C. Rath, D. B. Naik and S. K. Sarkar, Reversible growth of UO₂ nanoparticles in aqueous solutions through 7MeV electron beam irradiation, *J. Nucl. Mater.*, 2013, **438**, 26–31.
- 61 D. Hudry, C. Apostolidis, O. Walter, T. Gouder, E. Courtois, C. Kübel and D. Meyer, Non-aqueous Synthesis of Isotropic and Anisotropic Actinide Oxide Nanocrystals, *Chem. - A Eur. J.*, 2012, **18**, 8283–8287.
- 62 D. Hudry, C. Apostolidis, O. Walter, T. Gouder, E. Courtois, C. Kübel and D. Meyer, Controlled Synthesis of Thorium and Uranium Oxide Nanocrystals, *Chem. - A Eur. J.*, 2013, **19**, 5297–5305.
- 63 L. M. Moreau, A. Herve, M. D. Straub, D. R. Russo, R. J. Abergel, S. Alayoglu, J. Arnold, A. Braun, G. J. P. Deblonde, Y. Liu, T. D. Lohrey, D. T. Olive, Y. Qiao, J. A. Rees, D. K. Shuh, S. J. Teat, C. H. Booth and S. G. Minasian, Structural properties of ultra-small thorium and uranium dioxide nanoparticles embedded in a covalent organic framework, *Chem. Sci.*, 2020, **11**, 4648–4668.
- 64 D. L. Clark, M. P. Neu, W. Runde and D. W. Keogh, in *Kirk-Othmer Encyclopedia of Chemical Technology*, John Wiley & Sons, Inc., Hoboken, NJ, USA, 2006.
- 65 T. Gouder, R. Eloirdi and R. Caciuffo, Direct observation of pure pentavalent uranium in U₂O₅ thin films by high resolution photoemission spectroscopy, *Sci. Rep.*, 2018, **8**, 8306.
- 66 K. O. Kvashnina, S. M. Butorin, P. Martin and P. Glatzel, Chemical State of Complex Uranium Oxides, *Phys. Rev. Lett.*, 2013, **111**, 253002.
- 67 G. Leinders, R. Bes, J. Pakarinen, K. Kvashnina and M. Verwerft, Evolution of the Uranium Chemical State in Mixed-Valence Oxides, *Inorg. Chem.*, 2017, **56**, 6784–6787.
- 68 G. Leinders, R. Bes, K. O. Kvashnina and M. Verwerft, Local Structure in U(IV) and U(V) Environments: The Case of U₃O₇, *Inorg. Chem.*, 2020, **59**, 4576–4587.
- 69 L. Desfougeres, É. Welcomme, M. Ollivier, P. M. Martin, J. Hennuyer, M. O. J. Y. Hunault, R. Podor, N. Clavier and L. Favergeon, Oxidation as an Early Stage in the Multistep Thermal Decomposition of Uranium(IV) Oxalate into U₃O₈, *Inorg. Chem.*, 2020, **59**, 8589–8602.
- 70 S. D. Conradson, D. Manara, F. Wastin, D. L. Clark, G. H. Lander, L. A. Morales, J. Rebizant and V. V. Rondinella, Local Structure and Charge Distribution in the UO₂–U₄O₉ System, *Inorg. Chem.*, 2004, **43**, 6922–6935.
- 71 J. C. Renshaw, L. J. C. Butchins, F. R. Livens, I. May, J. M. Charnock and J. R. Lloyd, Bioreduction of Uranium: Environmental Implications of a Pentavalent Intermediate, *Environ. Sci. Technol.*, 2005, **39**, 5657–5660.
- 72 L. Amidani, T. V. Plakhova, A. Y. Romanchuk, E. Gerber, S. Weiss, A. Efimenko, C. J. Sahle, S. M. Butorin, S. N. Kalmykov and K. O. Kvashnina, Understanding the size effects on the electronic structure of ThO₂ nanoparticles, *Phys. Chem. Chem. Phys.*, 2019, **21**, 10635–10643.
- 73 R. Husar, R. Hübner, C. Hennig, P. M. Martin, M. Chollet, S. Weiss, T. Stumpf, H. Zänker and A. Ikeda-Ohno, Intrinsic formation of nanocrystalline neptunium dioxide under

- neutral aqueous conditions relevant to deep geological repositories, *Chem. Commun.*, 2015, **51**, 1301–1304.
- 74 A. Y. Romanchuk, T. V Plakhova, A. V Egorov, T. B. Egorova, P. V Dorovatovskii and Y. V Zubavichus, Redox-mediated formation of plutonium oxide nanoparticles, *Dalt. Trans.*, 2018, **47**, 11239–11244.
- 75 H. Geckeis, B. Grambow, A. Loida, B. Luckscheiter, E. Smailos and J. Quinones, Formation and Stability of Colloids under Simulated Near Field Conditions, *Radiochim. Acta*, 1998, **82**, 123-128.
- 76 H. Zänker and C. Hennig, Colloid-borne forms of tetravalent actinides: A brief review, *J. Contam. Hydrol.*, 2014, **157**, 87–105.